Super-Resolution GPS Receiver: User's Acceleration Computation

Yiran Luo
Department of Geomatics Engineering
University of Calgary
Calgary, Canada T2N 1N4
yiran.luo@ucalgary.ca

Li-Ta Hsu
Department of Aeronautical and Aviation Engineering
The Hong Kong Polytechnic University
Hung Hom, Hong Kong SAR, China
lt.hsu@polyu.edu.hk

Naser El-Sheimy
Department of Geomatics Engineering
University of Calgary
Calgary, Canada T2N 1N4
elsheimy@ucalgary.ca

***Abstract*— Current commercial global navigation satellite system (GNSS) receivers cannot measure the change of Doppler shift via baseband processing. However, positioning in challenging environments demands accurate Doppler estimates to replicate the actual intermediate-frequency (IF) line-of-sight (LOS) GNSS signals. Otherwise, the instantaneous GNSS measurements, like pseudoranges and carrier phases, will be seriously distorted, restricting the upper bound of GNSS positioning. This paper proposes a brand-new super-resolution (SR) GNSS receiver that computes the user's absolute acceleration based on super-long coherent integration (S-LCI), fractional Fourier transform (FRFT), and a baseband maximum likelihood estimator (MLE). A basic nonlinear least square (NLS) navigator taken as an intuitive example shows how the proposed receiver models and generates averaging Doppler rates via the baseband-dependent gradient descent (GD) algorithm. A global positioning system (GPS) software-defined radio (SDR) processing the L5 IF data collected via a mobile cart in the real world validates the proposed technique with the Doppler rate measurement, the user's acceleration navigation solution, and the clock drift rate.**

Keywords—super-long coherent integration (S-LCI), fractional Fourier transform (FRFT), Doppler rate measurement, super-resolution GNSS receiver, absolute acceleration, GPS L5 pilot, least square

I. INTRODUCTION

Current commercial GNSS receivers are unable to produce Doppler rate measurements. One reason is that the global navigation satellite system (GNSS) user's absolute acceleration is too weak to observe through the line-of-sight (LOS) signal Doppler [1]. Another reason resorts to the incomplete baseband signal processing techniques on which the current receivers depend [2]. More specifically, the coherent integration time used in current receivers (a typical value of 20 ms) is not long enough to recognize the change in the Doppler frequency of LOS GNSS signals in the baseband. [3]. Instead, a way to estimate such signal parameters relies on differencing between-epoch Doppler measurements or double-differencing the carrier phases [4], negatively introducing extra additive noise power to estimates that are not expected, especially in challenging environments.

As known, the Doppler frequency change is critical for carrier-based positioning techniques, such as cycle slip detection [5], so it would be desirable for one to accurately estimate it via the GNSS signal processing procedure. In that case, it avoids the unexpected noise power caused by the differencing operation, theoretically elevating the upper bound of the estimating accuracy of Doppler frequency change (or Doppler rate in the signal processing process), thereby tending to enhance the positioning performance potentially.

However, providing Doppler rate measurements via baseband processing manipulation is exceptionally challenging. First, current GNSS signal processing techniques are designed deeply and originally upon the conventional fast Fourier transform (FFT) concept and its frequency resolution limits the boundary of parameter estimation of unknown signals.

Second, today's hot debates on the GNSS community mainly focus on the data analysis of original GNSS measurements using state-of-the-art optimization algorithms [6] and integration with different types of sensor data [7], or adding antenna arrays to receivers [8], ignoring the importance of the breakthrough regarding GNSS baseband processing [9]–[11].

Third, the researchers and engineers of GNSS receivers are accustomed to the concept of finite impulse response (FIR) filtering (e.g., traditional loop filters) for devising an accurate tracking system, while the advantages of an infinite impulse response (IIR) method and extended coherent integration technique remain to dig in.

Finally, a thorough update for a brand-new GNSS receiver heavily depends on a reliable and easy-to-use platform which hugely hinders the development of baseband processing.

Then, as mentioned earlier, the Doppler rate of a single-channel GNSS satellite (a typical value is no more than 0.8 Hz/s [12]) is weak, avoiding fast and accurate estimation of this unknown parameter. It can be inferred that the estimating process will accelerate if less useful signal power is lost in the baseband processing. Extending the coherent integration time is a candidate for effectively preserving the carrier and code phase information, exploiting more LOS signal information in estimation. Nevertheless, it brings different problems in the baseband processing.

For instance, nuisance components such as high-order frequency terms (e.g., frequency rate or higher) due to the user's motion and low-quality oscillator variations will cause phase offset errors and hinder the success of super-long coherent integration (S-LCI) in the GNSS receivers. Recent works from Focal Point Positioning have addressed this issue by introducing a motion-compensated method in the baseband processing [13], [14].

In this study, we aim to identify an appropriate matched filter in the correlating process that can compensate for phase deviations exactly resulting from the change of LOS Doppler shifts. These Doppler shift changes (or Doppler rates)

2023 IEEE/ION Position, Location and Navigation Symposium (PLANS) | 978-1-6654-1772-3/23/$31.00 ©2023 IEEE | DOI: 10.1109/PLANS53410.2023.10140012

correspond to the frequency rate terms caused by the user's and satellite's motion accelerations/ decelerations and the local and satellite oscillator drift rates, among others. More specifically, the relationship between the Doppler rate match filter and the frequency rate terms resembles the counterpart between the classic Doppler frequency match filter (generated by the classic FFT) and the frequency shift terms (arise from various sources such as the user's and satellite's motion velocities, the local and satellite oscillator drifts, the changes in atmospheric delay, among others). Luckily, the digital fractional Fourier transform (FRFT) [15] can replace the FFT in baseband processing to simultaneously estimate the instantaneous Doppler shift and the averaging Doppler rate, enabling measuring Doppler rates to be possible.

Once the GNSS receivers obtain the Doppler rate measurements, the computation of the user's acceleration/ deceleration becomes an intriguing topic to explore. As we know, one of the challenges regarding this task is that the official interface control documents (ICDs) of GNSS do not offer the theory of calculating GNSS satellite accelerations.

Fortunately, a recent publication introduces the method of global positioning system (GPS) satellite acceleration computation with the broadcast navigation message in detail [16], which makes it possible to estimate the user's on-the-fly acceleration and the change of clock drifts with the proposed standalone SR GPS receivers.

According to the discussions above, we have access to obtaining the Doppler rate measurement and the satellite acceleration in a single channel through the proposed SR GPS receiver. Finally, like the absolute positions and clock bias errors solved via the pseudorange measurements or the absolute velocities and clock drift errors via the Doppler measurements [2], it is possible to build a system model to estimate the absolute accelerations/ decelerations and clock drift rates.

Accordingly, this paper aims to use an SR baseband maximum likelihood estimator (MLE) to measure the Doppler rate for GPS receivers based on a S-LCI technique and closed-form digital FRFT.

In summary, we aim to design an SR GPS receiver based on a baseband MLE and the S-LCI in the fractional Fourier domain (FRFD) [17] that can output Doppler rate measurements and compute the user's absolute acceleration/deceleration and the clock drift rate. Then, the main contributions of this work focuses on the following:

1. Compensate for the carrier phase curvature over the S-LCI procedure with the 2nd-order Keystone transform (KT) technique and generate a brand-new Doppler rate measurement by leveraging the state-of-the-art GNSS baseband techniques, i.e., the SR baseband MLE and the gradient descent (GD) optimization proposed by the authors' recent research [17];
2. Add the computation process of satellite accelerations/ decelerations to the proposed SR GPS SDR;
3. Design a prototype for the proposed SR GPS SDR where the system models will be built to estimate the user's absolute acceleration/ deceleration and local clock drift rate using the nominated Doppler rate measurements and satellite accelerations/ decelerations.
4. Implement the real-world experiments to validate the proposed SR GPS SDR prototype.

Finally, TABLE I. and TABLE II. compare the proposed SR GPS receiver and the traditional/ current commercial GPS receivers from the perspectives of GNSS measurements and GNSS navigation solutions, respectively, where the "NLS," "NCO," "SPP," "RTK," and "PPP" represent nonlinear least square, numerically controlled oscillator, single point positioning, real-time kinematic, and precise point positioning, respectively.

TABLE I. COMPARISON OF THE PROPOSED SR GNSS RECEIVER AND CURRENT COMMERCIAL (TRADITIONAL) RECEIVERS REGARDING GNSS MEASUREMENT GENERATION VIA INTERMEDIATE-FREQUENCY BASEBAND PROCESSING.

GNSS Measurement	Proposed SR receiver	Traditional/ commercial receiver
Pseudorange	Instantaneous (via NCO + **GD + analytic model prediction**)	Instantaneous (via NCO)
Carrier phase	Instantaneous (via NCO + **GD + analytic model prediction**)	Instantaneous (via NCO)
Doppler frequency/shift	Instantaneous (via GD + **analytic model prediction**)	Averaging (via GD)
Doppler (frequency/shift) rate	**Averaging (via GD)**	N/A

TABLE II. COMPARISON OF THE PROPOSED SR GNSS RECEIVER AND CURRENT COMMERCIAL (TRADITIONAL) RECEIVERS REGARDING GNSS NAVIGATION SOLUTION COMPUTATION.

GNSS navigation solution	Proposed SR receiver	Traditional/ commercial receiver
Absolute position	Yes (SPP/RTK/PPP)	Yes (SPP/RTK/PPP)
Absolute velocity	Yes (NLS update)	Yes (NLS update)
Absolute acceleration/ deceleration	**Yes (NLS update)**	N/A

II. CORE TECHNIQUES OF THE PROPOSED SR GPS RECEIVER

Commercial GNSS receivers commonly adopt a rate of 1 Hz to update data (e.g., GNSS measurements or positioning, velocity, and timing results) in mobile navigation. However, a typical value of baseband tracking loop rates can be up to 1000 Hz (when the coherent integration is set as 1 ms), which is much higher than the one a user's end demands.

Uniquely, the coherent processing interval of the proposed baseband technique allows a combined optimization of 1-s correlating outputs through the GD algorithm within a one-epoch interval and offers snapshot navigation solutions. In that case, the subtle averaging change of the Doppler shift between the actual and the received GNSS signals, which cannot be estimated from the regular tracking technique, can be obtained from the SR baseband MLE of the proposed SR receiver.

Finally, the NLS navigator of the receiver leverages the Doppler frequency change (or the Doppler rate)

measurements and their predictions to compute the user's absolute acceleration/ deceleration solutions.

A. Signal model for the S-LCI implementation

A 1-s S-LCI interval is used in the proposed SR SDR technique regarding the discussions above. However, a 1-s S-LCI interval is insufficient to match the exact Doppler rate value caused by the motion between the satellite and the GNSS receiver antenna along the LOS direction due to the low resolution of the matched filter in the FRFD. The inconsistency will lead to the consequences of power loss in the correlating process, unexpectedly causing the low estimation accuracy of received signal parameters.

Based on the authors' previous publications [18], [19], leveraging the analytic formula of the S-LCI correlator outputs in the FRFD can overcome the challenges of low resolution by compensating for the power loss through an MLE and GD optimization [17]. To maintain more correlation power over the S-LCI implementation, ignoring the data bit, a more accurate received GPS signal model at the intermediate frequency (IF) can be built as

$$\begin{aligned} s(t) = {} & 2aC\left(t - \tau_{PRN} + \tau_{dyn}(t)\right) \\ & \times \cos\left(2\pi f_I t + \left(\phi_I + \phi_{dyn}(t)\right)\right) \end{aligned} \tag{1}$$

with

$$\begin{aligned} \tau_{dyn}(t) &\triangleq \left(vt + \frac{\beta}{2}t^2\right)c^{-1} \\ \phi_I &\triangleq \phi_i - 2\pi(f_r + f)\tau_{PRN} \\ f &\triangleq f_r c^{-1} v \\ \mu &\triangleq f_r c^{-1}\beta \\ \phi_{dyn}(t) &\triangleq 2\pi(f_r + f)\tau_{dyn}(t) \\ &= 2\pi\frac{(f_r + f)}{f_r}ft + \pi\frac{(f_r + f)}{f_r}\mu t^2 \end{aligned} \tag{2}$$

where a is the baseband signal amplitude; t is the continuous time variable; $C(t)$ is the spreading code model; f_I is the IF; ϕ_I is the initial carrier phase at the IF and ϕ_i is the initial carrier phase excluding the term related to the propagation delay; τ_{PRN} denotes the propagation delay at the time of signal emission; $\tau_{dyn}(t)$ is the residual of the propagation delay related to signal dynamics along the LOS direction and $\phi_{dyn}(t)$ is the carrier phase change varying with the propagation delay residual due to the dynamics along the LOS direction; v is the equivalent velocity in m/s of the initial Doppler shift f in Hz and β is the equivalent acceleration in $\mathrm{m/s^2}$ of the averaging change of the Doppler shift μ (i.e., the Doppler rate) in Hz/s; f_r is the radio frequency and c is the speed of light.

Next section will address a range curvature issue of the actual carrier phase (2) and then, propose a method to solve it.

B. Carrier phase curvature compensation over the S-LCI correlation based on the 2nd-order KT

In this section, we will leverage a 2nd-order KT to compensate for the range (or carrier phase in this work) curvature over the S-LCI implementation. The phenomenon occurs in both the carrier and code phase terms over the S-LCI correlation due to the clock instability and the motion between the satellites and the receiver antenna [20]. As the case of the code phase is similar to the carrier phase, the following discussion will not mention the code phase compensation.

For simplicity, ignoring the components of the baseband signal amplitude a and the spreading code $C(t)$, the carrier signal is easy to be transferred to a complex form after an analytic Hilbert transform, i.e.,

$$s_{carr}(t) = e^{j\left(2\pi f_I t + 2\pi\frac{(f_r+f)}{f_r}ft + \pi\frac{(f_r+f)}{f_r}\mu t^2 + \phi_I\right)} \tag{3}$$

where it can be found that the carrier phase, i.e., the two terms $2\pi\frac{(f_r+f)}{f_r}ft$ and $\pi\frac{(f_r+f)}{f_r}\mu t^2$ related to the actual Doppler shift and rate, are coupled with the term $\frac{(f_r+f)}{f_r}$, causing the so-called range walk and range curvature (or quadratic range migration) to the instantaneous carrier phase. This phenomenon is always ignored in a traditional receiver (using a 1-to-20-ms coherent correlation), but it will cause the long coherent correlation power reduced. So, it needs compensating. Thus, a 2nd-order KT is used to cope with the range curvature issue, of which the mathematical model is expressed as follows

$$t = \sqrt{\frac{f_r}{f_r + f}}\,t' \tag{4}$$

where t' denotes the rescaled time variable. A GNSS baseband processor uses an NCO to replicate the local signal at the IF, so that the 2nd-order KT is implemented by rescaling the carrier NCO frequency as

$$\hat{f}'_{\phi,nco,n_C+1} = f_I + \hat{f}'_{n_C} \tag{5}$$

with

$$\hat{f}'_{n_C} = \sqrt{\frac{f_r + \hat{f}_{n_C}}{f_r}}\,\hat{f}_{n_C}$$

where $\hat{f}_{n_C}$ and $\hat{f}'_{n_C}$ represents the estimated Doppler shift via the SR baseband MLE before and after compensation, respectively, and subscript n_C denotes the index of the S-LCI correlation sequence. Next, executing the Fourier transform for $s_{carr}(t)$ at the one-matched-filter frequency of $\hat{f}'_{\phi,nco,k+1}$ within an interval of T_S (that is a slow-time coherent correlating process) at the slow-time interval (or resampling point) index n_S to (3) yields

$$\begin{aligned} &\chi[n_S](\hat{f}'_{n_C}) \\ &= \frac{1}{T_S}\int_{t+(n_S-1)T_S}^{t+n_S T_S} s_{carr}(t_x)e^{-j2\pi\hat{f}'_{\phi,nco,n_C+1}t_x}\,dt_x \\ &= \frac{1}{T_S}\int_{t+(n_S-1)T_S}^{t+n_S T_S} e^{j\left(2\pi\left(\frac{f_r+f}{f_r}f - \sqrt{\frac{f_r+\hat{f}_{n_C}}{f_r}}\hat{f}_{n_C}\right)t_x + \pi\frac{f_r+f}{f_r}\mu t_x^2 + \phi_I\right)}dt_x \\ &= \frac{1}{T_S}\sqrt{\frac{f_r}{f_r+\hat{f}_{n_C}}}e^{j\phi_I} \\ &\times \int_{\sqrt{\frac{f_r+\hat{f}_{n_C}}{f_r}}(t+(n_S-1)T_S)}^{\sqrt{\frac{f_r+\hat{f}_{n_C}}{f_r}}(t+n_S T_S)} e^{j\left(2\pi\left(\frac{f_r+f}{f_r}\sqrt{\frac{f_r}{f_r+\hat{f}_{n_C}}}f - \hat{f}_{n_C}\right)t'_x + \pi\frac{f_r+f}{f_r+\hat{f}_{n_C}}\mu(t'_x)^2\right)}dt'_x \\ &\approx \frac{1}{T_S}\sqrt{\frac{f_r}{f_r+\hat{f}_{n_C}}}e^{j\phi_I}\int_{\sqrt{\frac{f_r+\hat{f}_{n_C}}{f_r}}(t+(n_S-1)T_S)}^{\sqrt{\frac{f_r+\hat{f}_{n_C}}{f_r}}(t+n_S T_S)} e^{j(2\pi\Delta f' t'_x + \pi\mu(t'_x)^2)}dt'_x \end{aligned}$$

with

$$\Delta f' \triangleq \sqrt{\frac{f_r+f}{f_r}}f-\hat{f}_{nc}, t_x=\sqrt{\frac{f_r}{f_r+\hat{f}_{nc}}}t'_x$$

In the GNSS baseband tracking, a carrier NCO can be further used to update the initial carrier phase and the procedure is expressed as follows

$$\begin{aligned}&\chi'[n_S]\left(\hat{f}'_{nc}\right)\\&=e^{-j\hat{\phi}_I}\chi[n_S]\left(\hat{f}'_{nc}\right)\\&=e^{j\Delta\phi}\frac{1}{T_S}\sqrt{\frac{f_r}{f_r+\hat{f}_{nc}}}\\&\times\int_{\sqrt{\frac{f_r+\hat{f}_{nc}}{f_r}}(t+(n_S-1)T_S)}^{\sqrt{\frac{f_r+\hat{f}_{nc}}{f_r}}(t+n_ST_S)}e^{j2\pi\Delta f' t'_x+j\pi\mu\left(t'_x\right)^2}dt'_x\end{aligned}\quad (6)$$

with

$$\Delta\phi \triangleq \phi_I-\hat{\phi}_I$$

where it can be observed that the range curvature term $\pi\frac{f}{f_r}\mu t^2$ as mentioned in (3) has been removed.

C. Doppler rate compensation over the S-LCI correlation based on the digital FRFT

Carrier phase migration caused by the Doppler rate (i.e., the Doppler frequency migration), that is, $\pi\mu(t'_x)^2$ in the $\chi'[n_S]\left(\hat{f}'_{nc}\right)$ model (6), will be compensated by the digital FRFT which has been introduced in detail in [17] where a complete GNSS signal model is considered. The decision-making process can be expressed as

$$\left[\hat{\tau},\hat{f},\hat{\mu},\hat{\phi}\right]=\text{argmax}\left\{\left|DF^p\left\{\tilde{\chi}^+[n_S]\left(\hat{f}'_{nc}\right)\right\}\right|\right\}\quad (7)$$

with

$$\chi^+[n_S]=R_{cc}[n_S]\chi'[n_S]\left(\hat{f}'_{nc}\right)$$

where $\tilde{\chi}^+[n_S]\left(\hat{f}'_{nc}\right)$ is the measured slow-time GNSS correlation sequences in the baseband and $\chi^+[n_S]$ is the expression without noise; $R_{cc}[n_S]$ denotes the S-LCI amplitude related to code auto-correlation function varying with the code offset; $DF^p\{\cdot\}$ represents the digital FRFT operator tuned by the FRFT order p (corresponding to the Doppler rate); $\hat{\tau}$, $\hat{f}$, $\hat{\phi}$, and $\hat{\mu}$ denote the matched code delay, Doppler frequency, carrier phase and Doppler rate, respectively, with the digital FRFT over the S-LCI interval.

The closed-form expression for the S-LCI correlation in the FRFD, that is, the output of $DF^p\left\{\chi^+[n_S]\left(\hat{f}'_{nc}\right)\right\}$ is given as the following

$$\begin{aligned}\chi_b^+=&\sqrt{1-j\cot\left(\frac{\pi}{2}p\right)}\\&\times e^{j\pi\frac{\left(\Delta f'+\frac{\mu}{2}N_ST_S\right)^2\cot\left(\frac{\pi}{2}p\right)}{N_S}}\\&\times e^{j\left(\Delta\phi+\pi\Delta f' N_ST_S+\frac{\pi}{4}\mu N_S^2T_S^2\right)}|\chi_b^+|\end{aligned}\quad (8)$$

with

$$|\chi_b^+| \triangleq aR_\Sigma\kappa_1^f\kappa_2^f\kappa_2^\mu$$

where N_S is the total number of the slow-time correlation over an S-LCI interval; the closed-form correlation amplitude $|\chi_b^+|$ and the remained carrier phase terms have been introduced in details in the authors' previous research [17], [19].

Finally, an SR baseband MLE based on the (8) (see [17]) can be formed to further optimize the matched Doppler rate $\hat{\mu}$ via the digital FRFT (see (7)) giving the final Doppler rate measurement $\tilde{\mu}$.

The baseband data $\tilde{\mu}$ is a brand-new GNSS measurement concerning the current GNSS community, and it can be used to compute the absolute acceleration and the local clock drift rate which will be introduced in the subsequent sections.

D. Computation of satellite acceleration

Undoubtedly, estimation of the user's acceleration/clock drift rate requires the accurate satellite acceleration provided in the GPS ICDs.

Reference [16] provides a detailed methodology for the computation of GPS satellite velocity and acceleration using the broadcast navigation message, offering an opportunity to estimate the user's acceleration on the receiver end. Therefore, this work adds the satellite acceleration computation to the proposed SDR and it will not be stated in this paper anymore.

E. Computation of the user's absolute acceleration and clock drift rate using the NLS method

A user's position and clock bias error are traditionally computed and optimized from the coarse initial 3D position coordinates using NLS regression. No less than four satellites (considering a single constellation) are demanded to estimate four unknowns. The user's acceleration computation resembles the position calculation except for the measurements (Doppler rates generated via the baseband processing as introduced earlier) and unknown states (user's accelerations and clock drift rate).

The computation of the brand-new navigational solutions (that is the 3D-space user's absolute acceleration and the clock drift rate) will be introduced subsequently for the integrity of this paper.

At first, a pseudorange model ρ^j can be expressed as

$$\rho^j \triangleq r^j+c\delta t_r-c\delta t^j+B^j_{\rho,atm}+\varepsilon^j_\rho\quad (9)$$

where the superscript j denotes the satellite number; r^j is the geometry distance, δt_r is the local clock bias error, δt^j is the satellite clock bias error, $B^j_{\rho,atm}$ is the atmospheric delay error, and ε^j_ρ is the remained pseudorange random error.

Then, the derivative of (9) with respect to the time variable yielding the pseudorange rate $\dot{\rho}^j$ can be modeled as

$$\dot{\rho}^j \triangleq \dot{r}^j+c\delta\dot{t}_r-c\delta\dot{t}^j+\varepsilon^j_{\dot{\rho}}\quad (10)$$

where $\delta\dot{t}_r$ and $\delta\dot{t}^j$ are the local and satellite clock drift errors, $\varepsilon^j_{\dot{\rho}}$ is the remained pseudorange rate random error, the change rate of the atmospheric delay error is not significant so that it is omitted in this model, $\dot{r}^j$ is the change rate of the geometry distance.

Analogously, the 2nd-order pseudorange rate (i.e., the change of the pseudorange rate) $\ddot{\rho}^j$ can be modeled via the derivative of (10) with respect to the time variable, that is,

$$\ddot{\rho}^j \triangleq \ddot{r}^j + c\delta\ddot{t}_r + \varepsilon_{\ddot{\rho}}^j \tag{11}$$

where $\delta\ddot{t}_r$ denotes the local clock drift rate (i.e., the change rate of the clock drift error), $\varepsilon_{\ddot{\rho}}^j$ is the remained 2nd-order pseudorange rate random error (including the error source due to the centrifugal acceleration [21]), $\ddot{r}^j$ is the 2nd-order range rate (i.e., the change of the geometry distance rate) which has a relationship with the user's and satellite's acceleration in the Earth-centered Earth-fixed (ECEF) coordinate frame, i.e.,

$$\ddot{r}^j \triangleq (\boldsymbol{a}^j - \boldsymbol{a}) \cdot \boldsymbol{l}^j \tag{12}$$

with

$$\boldsymbol{a} \triangleq \begin{bmatrix} \ddot{x} \\ \ddot{y} \\ \ddot{z} \end{bmatrix}$$

where $\boldsymbol{a}^j$ and $\boldsymbol{a}$ are the satellite acceleration and the user's acceleration vectors in the ECEF frame, respectively, $(\cdot)$ is an inner product operator; $\boldsymbol{l}^j$ is the unit direction cosine vector with respect to the satellite j. After that, combining (11) and (12), an equation can be formed as

$$\boldsymbol{H}\Delta\ddot{\boldsymbol{x}} = \ddot{\boldsymbol{b}} + \boldsymbol{\varepsilon}_{\ddot{\rho}}$$

with

$$\ddot{\boldsymbol{b}} \triangleq \begin{bmatrix} -\lambda\tilde{\mu}^{(1)} - \ddot{r}^{(1)} - c\delta\ddot{t}_r \\ -\lambda\tilde{\mu}^{(2)} - \ddot{r}^{(2)} - c\delta\ddot{t}_r \\ \vdots \\ -\lambda\tilde{\mu}^{(L)} - \ddot{r}^{(L)} - c\delta\ddot{t}_r \end{bmatrix}$$

$$\Delta\ddot{\boldsymbol{x}} \triangleq \begin{bmatrix} \Delta\ddot{x} \\ \Delta\ddot{y} \\ \Delta\ddot{z} \\ c\Delta\delta\ddot{t}_r \end{bmatrix} \triangleq \begin{bmatrix} \ddot{x} - \ddot{x}_0 \\ \ddot{y} - \ddot{y}_0 \\ \ddot{z} - \ddot{z}_0 \\ c\left(\delta\ddot{t}_r - \delta\ddot{t}_{r,0}\right) \end{bmatrix}$$

$$\boldsymbol{H} \triangleq \begin{bmatrix} -\left(\boldsymbol{l}^{(1)}\right)^T & 1 \\ -\left(\boldsymbol{l}^{(2)}\right)^T & 1 \\ \vdots & \vdots \\ -\left(\boldsymbol{l}^{(L)}\right)^T & 1 \end{bmatrix}, \boldsymbol{\varepsilon}_{\ddot{\rho}} \triangleq \begin{bmatrix} \varepsilon_{\ddot{\rho}}^{(1)} \\ \varepsilon_{\ddot{\rho}}^{(2)} \\ \vdots \\ \varepsilon_{\ddot{\rho}}^{(L)} \end{bmatrix}$$

where $\ddot{\boldsymbol{b}}$, $\Delta\ddot{\boldsymbol{x}}$, $\boldsymbol{H}$, and $\boldsymbol{\varepsilon}_{\ddot{\rho}}$ represent the closed-form measurement vector, state error vector, design matrix and random error vector, respectively; superscript values $\{(1), (2), \ldots (L)\}$ denotes the set of channel indexes where L is the total channel number; subscript 0 denotes the initial or the previously iterative state estimates; $\ddot{x}$, $\ddot{y}$, and $\ddot{z}$ are the user's acceleration navigation solutions of the respective three directions with respect to the ECEF frame; $\tilde{\mu}^{(L)}$ is the averaging Doppler rate measurements generated through the SR baseband MLE based on the S-LCI in the FRFD (as described in Section II-C), λ is the wavelength of the radio signalFinally, a standard NLS is leveraged to estimate the user's acceleration and the clock drift rate as follows

$$\Delta\hat{\ddot{\boldsymbol{x}}} = \left(\hat{\boldsymbol{H}}^T\hat{\boldsymbol{H}}\right)^{-1}\hat{\boldsymbol{H}}^T\hat{\ddot{\boldsymbol{b}}}$$

$$\hat{\ddot{\boldsymbol{x}}} = \hat{\ddot{\boldsymbol{x}}}_0 + \Delta\hat{\ddot{\boldsymbol{x}}}$$

where $\hat{\boldsymbol{H}}$ is computed with the unit vector $\hat{\boldsymbol{l}}^{(L)}$ from the *a priori* position to the satellite; $\hat{\ddot{\boldsymbol{b}}}$ is obtained from the clock drift rate error prediction $\delta\hat{\ddot{t}}_r$ and the 2nd-order pseudorange rate $\hat{\ddot{r}}^{(L)}$ predicted by

$$\hat{\ddot{r}}^{(L)} = \left(\hat{\boldsymbol{a}}^{(L)} - \begin{bmatrix} \hat{\ddot{x}}_0 \\ \hat{\ddot{y}}_0 \\ \hat{\ddot{z}}_0 \end{bmatrix}\right) \cdot \hat{\boldsymbol{l}}^{(L)} \tag{13}$$

where $\hat{\boldsymbol{a}}^{(L)}$ is the satellite acceleration in the ECEF frame which is computed through the ephemeris and the method has been introduced in Section II-D; $\left[\hat{\ddot{x}}_0, \hat{\ddot{y}}_0, \hat{\ddot{z}}_0\right]^T$ is the *a priori* acceleration vector. Ultimately, $\hat{\ddot{\boldsymbol{x}}}$ is the estimated state vector including the x-, y-, z- user's absolute acceleration and the clock drift rate and it is updated via the GD optimization.

III. Real-World Experiment Validation

The real-world GPS IF data were collected on the campus at the University of Calgary. The testing environment and the experimental setup are given in Figure 1. A NovAtel antenna receives all-bands radio frequency GNSS signal. A Fraunhofer GNSS frontend (where the sampling rate is 40.5 MHz for the L5 band signals with the complex 8-bit quantization) and a u-blox MAX-M10S processed the GNSS data from the same antenna via a splitter. And, the MAX-M10S receiver was integrated with the Xsens MTi-670 IMU to offer the GNSS/IMU integrated velocity reference (which can be differenced to output the user's acceleration reference in the local-level frame). All the experimental devices and equipment are set on the top of a small cart used to carry out a kinematic field test.

Then, the proposed algorithm is realized in a GPS software-defined radio (SDR) where the IF GNSS signals collected from the Fraunhofer GNSS frontend were processed and output the proposed Doppler rate measurements and GNSS user's absolute acceleration solutions. Both traditional tracking algorithms and commercial solution references are compared with the proposed solutions. More details will be discussed subsequently.

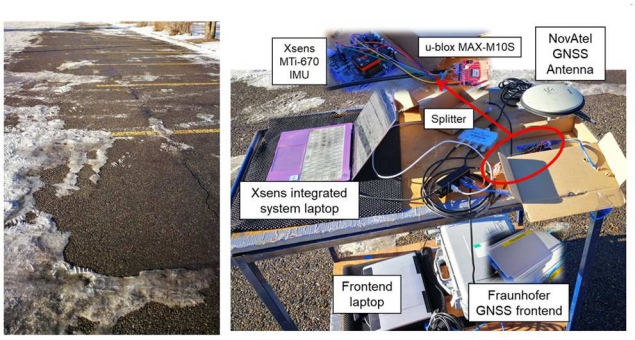

Figure 1 Testing ground environment (left) and experimental setup (right).

The pilot channel of the GPS L5 signals (i.e., GPS L5Q) were used to implement S-LCI implementation and produce the proposed Doppler rate measurements. Besides, the data channel of the GPS L5 signals (i.e., GPS L5I) are processed at the IF to extract the transmit time which is used by the L5Q IF data to generate the pseudorange measurements such that an absolute position solution can be solved based on the L5Q signals and it will be used to calculate the unit cosine vector $\hat{\boldsymbol{l}}^{(L)}$ to predict the 2nd-order pseudorange rate in (13).

It is also worth emphasizing that other types of GNSS signals are also available for the proposed algorithm of this work. The purpose of using the GPS L5Q signals in this experiment is for simplicity, as the procedure of data-bit stream wipe-off can be omitted. However, the Doppler

frequency of GPS L5 band signals will significantly impact baseband signal processing more than the old GPS signals like L1 C/A, which may cause a reduced signal estimation accuracy.

Therefore, the sky plot of the used GPS L5 satellites is illustrated in Figure 2 (top) where the C/N0 condition based on the proposed SR baseband MLE technique of each satellite is also expressed with the color map. Moreover, the tested trajectory generated from the GNSS/IMU integrated positioning solutions is plotted in Google Map as shown in Figure 2 (bottom) where the corresponding velocity along the trajectory is also depicted with the color map. And a list describing the used GNSS SDR algorithms and commercial receiver reference is given in TABLE III.

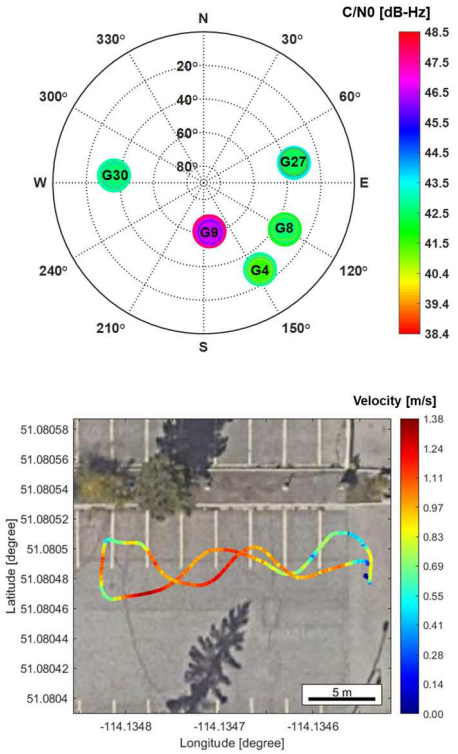

Figure 2 Sky plot of the used GPS L5 satellites with the C/N0 color map (top) and tested trajectory in Google Map with the velocity color map (bottom).

TABLE III. DESCRIPTION OF THE TESTED SDR ALGORITHMS AND COMMERCIAL REFERENCE IN THE REAL-WORLD EXPERIMENT.

Receiver Type	Description
20ms pll	GPS L5Q signals; traditional 3rd-order PLL with 18-Hz bandwidth; pure PLL discriminator, 20-ms coherent integration [2]
mle (no ktt)	GPS L5Q signals; proposed acceleration/clock drift rate computation in this work **excluding the KT technique (KTT)** (i.e., Section II-B) (SR baseband MLE + 1-s S-LCI)
proposed mle (ktt)	GPS L5Q signals; proposed acceleration computation/clock drift rate in this work **including the KTT** (SR baseband MLE + 1-s S-LCI)
Xsens ref	GPS / QZSS L1C/A + Galileo E1B/C + GLONASS L1OF signals (u-blox MAX-M10S); Xsens MTi-670 GNSS/IMU integrated velocity and velocity difference (acceleration) references

First, the velocity estimation from the GPS L5Q Doppler measurements produced with the traditional PLL algorithms are provided in Figure 3. The traditional estimated curves are compared with the Xsens GNSS/IMU integrated velocity reference to show the availability of the received GPS L5 IF data for navigation solutions. It can be found that the velocity curves in the horizontal plane obtained from the GPS L5Q SDR are consistent with the reference.

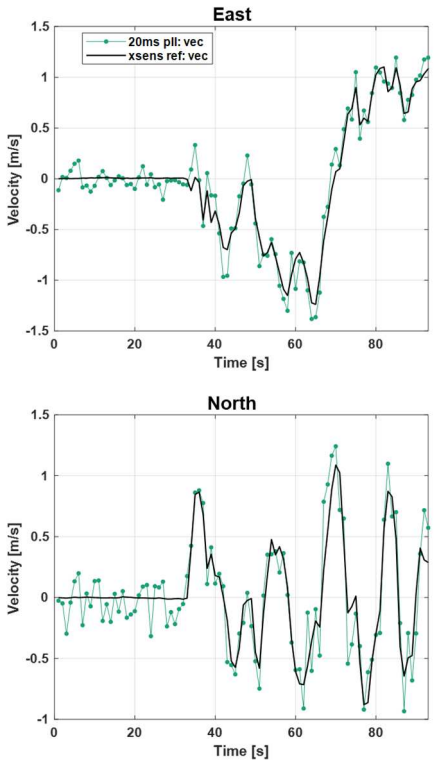

Figure 3 Velocity computation curves based on a traditional PLL GPS L5Q SDR compared to the commercial reference.

So, it can be proved that the received GPS L5 IF data can be further used for the Doppler rate generation and user's acceleration computation with the proposed algorithms in this work. The following contents will assess the Doppler rate quality as well as the accuracy of the acceleration and clock drift rate estimates.

It is worth noting that this work primarily focuses on the absolute acceleration computation and its measurement generation technique. In that case, the navigational velocity and position solutions and the related Doppler shift and pseudorange measurements quality based on the SR baseband MLE technique will not be discussed here. But parts of the contents have been investigated in our earlier paper and more contents will be completed in our future research.

To show the improvement of the MLE baseband technique compared to the traditional tracking results, Figure 4 plots the between-epoch double-difference (DD) curves of the traditional carrier phase measurements in comparison with the proposed Doppler rate measurement curves in the same figure for the five used GPS L5 satellites.

Based on the estimates from the first 30-second static testing data, one can easily find that the biased error of the Doppler rate from all the used satellites has been reduced compared to the traditional PLL tracking results. But it is difficult to say how it improves the user's solutions in a kinematic scenario.

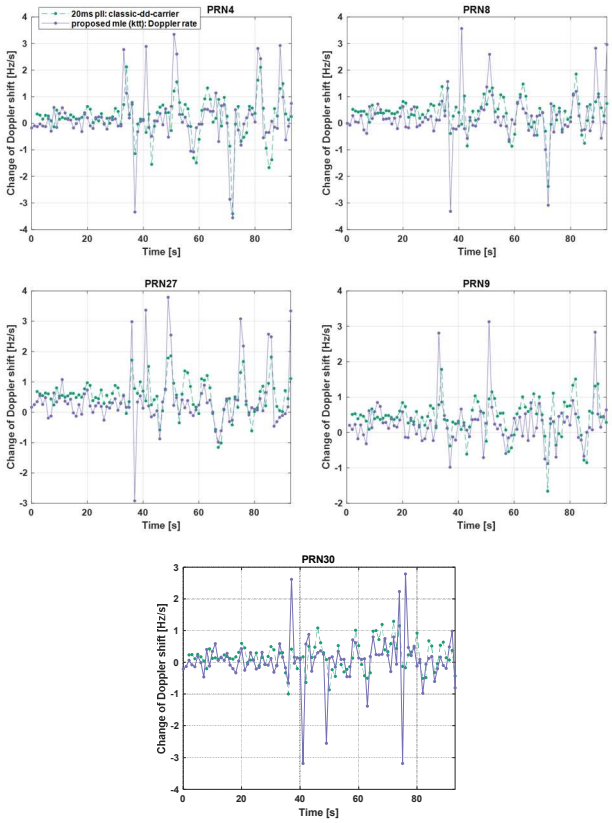

Figure 4 Comparison of the proposed Doppler rate estimation (averaging) and the DD carrier phase measurements generated from the traditional PLL (instantaneous).

Under this circumstance, navigation solutions in terms of the user's acceleration and the clock drift rate will be computed so that the navigation reference from a commercial system can be used to evaluate the proposed algorithm in a kinematic scenario.

Based on the earlier discussions, we further compare three SDR acceleration navigation results including the traditional and the proposed ones in Figure 5. The traditional PLL tracking cannot compute the absolute acceleration, so the velocity difference is computed for the traditional solutions, and they are plotted in the same figure with the proposed absolute acceleration solutions for an equivalent evaluation.

Obviously, the traditional navigation results produce much more noise than the ones from the two SR baseband MLE SDRs along all the eastern, northern, and vertical directions except for several outliers. In other words, the proposed acceleration computation technique has proved to efficiently de-noise the unexpected dynamic error when solving the navigation results.

Another phenomenon indicates that, regarding the moment the actual acceleration changes, the proposed SDR technique is more likely to cause a larger acceleration error compared to the traditional results. The reason is that the previous 1-s acceleration estimates can affect the current 1-s estimating process implying an inferior acceleration solution when the user's maneuverability is high at the transition moment of the two seconds.

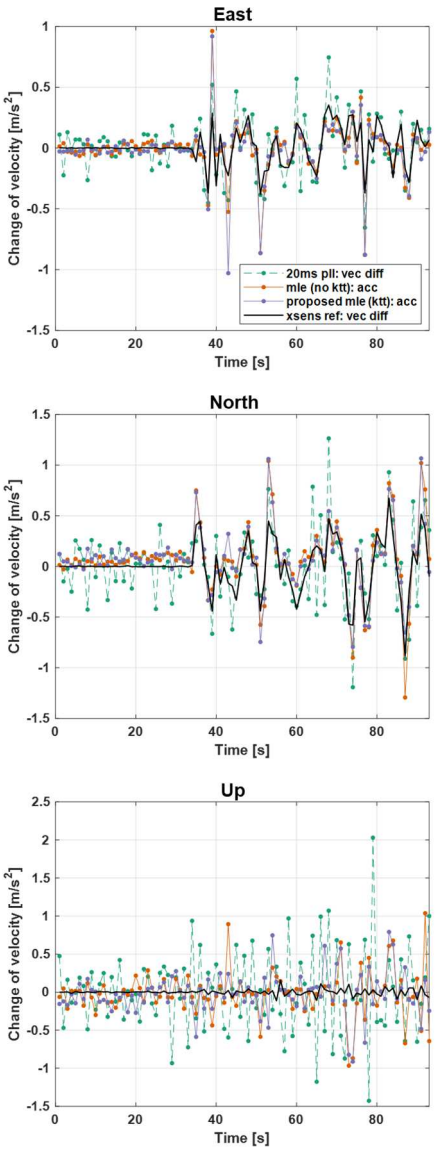

Figure 5 Comparison of the proposed user's acceleration (proposed) or change of velocity (traditional/ commercial) estimation.

In other words, the proposed SDR can have a more extraordinary improvement on the measurement quality in the scenario when the user's acceleration does not change very fast, such as the autonomous driving situation which will be tested in our future work. But if the acceleration-level measurements and solutions from the proposed SDR are integrated with the acceleration-level data from an inertial sensor, the maneuverability can be significantly enhanced. This is a new application in the GNSS community which our future research will investigate as well.

Furthermore, it can be seen from Figure 5, that the use of the 2nd-order KT technique can further improve the SDR performance and slightly increase the acceleration accuracy. Statistical analysis will be provided later for a more thorough discussion.

Besides of the absolute acceleration estimating performance, the absolute clock drift rate results are also assessed in Figure 6 where we, again, difference the clock drift estimates obtained from the traditional PLL as an equivalent comparison.

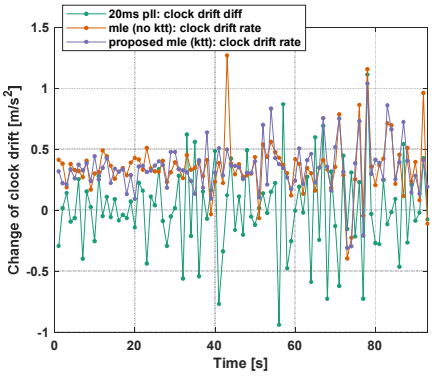

Figure 6 Comparison of the proposed clock drift rate (proposed) or change of clock drift (traditional/ commercial) estimation.

The result curve indicates that the proposed SDR has the potential to model the higher-order clock error with lower noise power. However, a biased error needs addressing before that. The reason may resort to the poor geometry of the satellites along the vertical direction, the sophisticated phase dynamics within an S-LCI interval that cannot be well matched with the FRFT implementation, and the non-compensated centrifugal acceleration mentioned earlier.

To show how much the 2nd-order KT technique can increase the accuracy of the proposed SR GPS SDR regarding the navigation solutions, the statistical analysis results and comparisons in terms of the absolute acceleration and clock drift rate estimation are listed in TABLE IV. and TABLE V.

TABLE IV. ACCURACY OF THE ABSOLUTE ACCELERATION AND CLOCK DRIFT RATE ESTIMATES

Method	**E**	**N**	**U**	**Clock drift rate**
	RMSE (2σ)[m/s^2]			***STD (2σ) [m/s^2]***
20 ms pll	0.140	0.233	0.481	N/A
mle (no ktt)	0.097	0.146	0.207	0.149
mle (ktt)	**0.093**	**0.132**	**0.186**	**0.145**

TABLE V. ACCURACY IMPROVEMENT OF THE 2ND-ORDER KT FOR 1-S S-LCI SR GPS SDR IN USER'S ABSOLUTE ACCELERATION AND CLOCK DRIFT RATE COMPUTATION

mle (ktt) improvement w.r.t.	**E**	**N**	**U**	**Clock drift rate**
20 ms pll	**From "N/A" to "available"**			
mle (no KT)	**4.64%**	**9.59%**	**10.18%**	**2.38%**

On the one hand, compared to the indirect estimation of the change of velocity from the traditional PLL, the proposed SDR can output the direct acceleration estimation in a much higher accuracy (i.e., the RMSE with a 2σ rule). It enables the proposed SDR based on the SR baseband MLE and the KT technique to open a new path computing the absolute acceleration that is not available for the traditional GNSS receiver.

On the other hand, when the 2nd-order KT technique is used to compensate for the carrier phase curvature over the baseband S-LCI implementation, the proposed GPS SDR navigation solution accuracy (i.e., the RMSE with a 2σ rule) has been improved by 4.64%, 9.59%, and 10.18% along the eastern, northern, and vertical directions, respectively; while the random noise power of the clock drift rate (i.e., the STD with a 2σ rule) has been reduced by 2.38%.

It is worthwhile to mention that the improvement regarding the KT compensation can be more apparent when the S-LCI interval is longer than one second and vice versus.

IV. CONCLUSIONS

In this paper, a technology about producing the Doppler rate measurements from a GPS L5 receiver and how to compute the user's acceleration and clock drift rate are proposed based on the techniques of the S-LCI implementation, the carrier phase compensation with the digital FRFT and the 2nd-order KT, the baseband processing using the MLE and GD, the satellite acceleration computation. Furthermore, the related experiments with the real-world data are implemented on a small mobile cart to validate the proposed standalone GPS navigation system. The conclusions are drawn as follows:

1. A new type of GNSS measurements, that is the averaging Doppler rate, has been generated from the baseband processor of the proposed SR GPS SDR with smaller biased errors compared to the traditional between-epoch double-difference carrier phase error;
2. The user's absolute acceleration results and the absolute clock drift rate have been successfully solved by the proposed SR GPS SDR while these solutions are not available in current commercial/ traditional GNSS receivers;
3. The proposed SR GPS SDR has improved the absolute acceleration by a maximum of 10.18% along the vertical direction when the 2nd-order KT technique is used to compensate for the 1-s S-LCI correlation in the FRFD.

As an outlook, a massive market regarding new navigation applications can be excavated through the brand-new GNSS Doppler rate measurements, the acceleration navigation solutions, and the clock drift rate estimation for timing, produced by the proposed SR GPS receiver in the future.

ACKNOWLEDGEMENT

This research was supported by funding provided to Professor Naser El-Sheimy from NSERC CREATE and Canada Research Chairs programs. The authors would like to extend sincere gratitude to Prof. Kyle O'Keefe and Prof. Yang Gao of the Department of Geomatics Engineering at the University of Calgary for generously granting us access to their experimental equipment in their labs.

REFERENCES

[1] N. S. Gowdayyanadoddi, A. Broumandan, J. T. Curran, and G. Lachapelle, "Benefits of an ultra stable oscillator for long coherent integration," in Proceedings of the ION GNSS+ 2014, Tampa, Florida, USA, Sep 8-12, 2014, pp. 1578–1594.

[2] E. D. Kaplan and C. Hegarty, Understanding GPS/GNSS. Principles and applications, 3rd ed. Artech house, 2017.

[3] Y. Luo, L.-T. Hsu, and Y. Pan, "A Super-Resolution Algorithm with FRFT Towards GNSS TOA Estimation for Multipath Channel," in Proceedings of the ION GNSS+ 2021, St. Louis, Missouri, USA, Sep 20-24, 2021, pp. 3350–3359. doi: 10.33012/2021.17951.

[4] C. Cai, Z. Liu, P. Xia, and W. Dai, "Cycle slip detection and repair for undifferenced GPS observations under high ionospheric activity," GPS Solutions, vol. 17, no. 2, pp. 247–260, Apr. 2013, doi: 10.1007/s10291-012-0275-7.

[5] B. Li, Y. Qin, and T. Liu, "Geometry-based cycle slip and data gap repair for multi-GNSS and multi-frequency observations," J Geod, vol. 93, no. 3, pp. 399–417, Mar. 2019, doi: 10.1007/s00190-018-1168-5.

[6] T. Suzuki, “Time-Relative RTK-GNSS: GNSS Loop Closure in Pose Graph Optimization,” IEEE Robot Autom Lett, vol. 5, no. 3, pp. 4735–4742, Jul. 2020, doi: 10.1109/LRA.2020.3003861.

[7] K. W. Chiang, G. J. Tsai, H. W. Chang, C. Joly, and N. EI-Sheimy, “Seamless navigation and mapping using an INS/GNSS/grid-based SLAM semi-tightly coupled integration scheme,” Information Fusion, vol. 50, no. January, pp. 181–196, Oct. 2019, doi: 10.1016/j.inffus.2019.01.004.

[8] S. Daneshmand and G. Lachapelle, “Integration of GNSS and INS with a phased array antenna,” GPS Solutions, vol. 22, no. 1, p. 3, Jan. 2018, doi: 10.1007/s10291-017-0672-z.

[9] P. Closas and A. Gusi-Amigo, “Direct Position Estimation of GNSS Receivers: Analyzing main results, architectures, enhancements, and challenges,” IEEE Signal Process Mag, vol. 34, no. 5, pp. 72–84, Sep. 2017, doi: 10.1109/MSP.2017.2718040.

[10] P. D. Groves, Q. Zhong, R. Faragher, and P. Esteves, “Combining Inertially-aided Extended Coherent Integration (Supercorrelation) with 3D-Mapping-Aided GNSS,” in Proceedings of the ION GNSS+ 2020, Sep 21-25, Oct. 2020, pp. 2327–2346. doi: 10.33012/2020.17767.

[11] N. Krasner and P. McBurney, “Application of Super Resolution Correlation to Multipath Mitigation in an L5 Channel,” in Proceedings of the ION GNSS+ 2022, Denver, Colorado, USA, Sep 19-23, Oct. 2022, pp. 3249–3269. doi: 10.33012/2022.18584.

[12] F. S. T. Van Diggelen, A-GPS: Assisted GPS, GNSS, and SBAS. Boston&London: Artech House, 2009.

[13] R. Faragher, N. Couronneau, and R. M. Crockett, “Method and system for calibrating a system parameter,” US20220283322A1

[14] R. Faragher, N. Couronneau, R. M. Crockett, and P. Duffett-Smith, “Method, apparatus, computer program, chip set, or data structure for correlating a digital signal and a correlation code,” US10321430B2

[15] H. M. Ozaktas, O. Arikan, M. A. Kutay, and G. Bozdagt, “Digital computation of the fractional Fourier transform,” IEEE Transactions on Signal Processing, vol. 44, no. 9, pp. 2141–2150, 1996, doi: 10.1109/78.536672.

[16] B. F. Thompson, S. W. Lewis, S. A. Brown, and T. M. Scott, “Computing GPS satellite velocity and acceleration from the broadcast navigation message,” NAVIGATION, vol. 66, no. 4, pp. 769–779, Dec. 2019, doi: 10.1002/navi.342.

[17] Y. Luo, L.-T. Hsu, and N. El-Sheimy, “A Baseband MLE for Snapshot GNSS Receiver Using Super-Long-Coherent Correlation in a Fractional Fourier Domain,” NAVIGATION, vol. 70, no. 3, Apr. 2023, doi: 10.33012/navi.588.

[18] Y. Luo, L. Zhang, and H. Ruan, “An Acquisition Algorithm Based on FRFT for Weak GNSS Signals in A Dynamic Environment,” IEEE Communications Letters, vol. 22, no. 6, pp. 1212–1215, Jun. 2018, doi: 10.1109/LCOMM.2018.2828834.

[19] Y. Luo, C. Yu, S. Chen, J. Li, H. Ruan, and N. El-Sheimy, “A Novel Doppler Rate Estimator Based on Fractional Fourier Transform for High-Dynamic GNSS Signal,” IEEE Access, vol. 7, pp. 29575–29596, 2019, doi: 10.1109/ACCESS.2019.2903185.

[20] F. Zhou, R. Wu, M. Xing, and Z. Bao, “Approach for single channel SAR ground moving target imaging and motion parameter estimation,” IET Radar, Sonar & Navigation, vol. 1, no. 1, p. 59, 2007, doi: 10.1049/iet-rsn:20060040.

[21] L. Serrano, D. Kim, and R. B. Langley, “A Single GPS Receiver as a Real-Time, Accurate Velocity and Acceleration Sensor,” in Proceedings of the ION GNSS 2004, Long Beach, CA, USA, Sep 21 - 24, 2004, pp. 2021–2034.

.